Radio Astronomy Receivers/Detectors

Alan E. E. Rogers

MIT Haystack Observatory

3 April 2008

Talk and demonstration of a "simple radio interferometer" given to Prof. Paul Schechter's class on "Astronomical Instrumentation" at MIT.

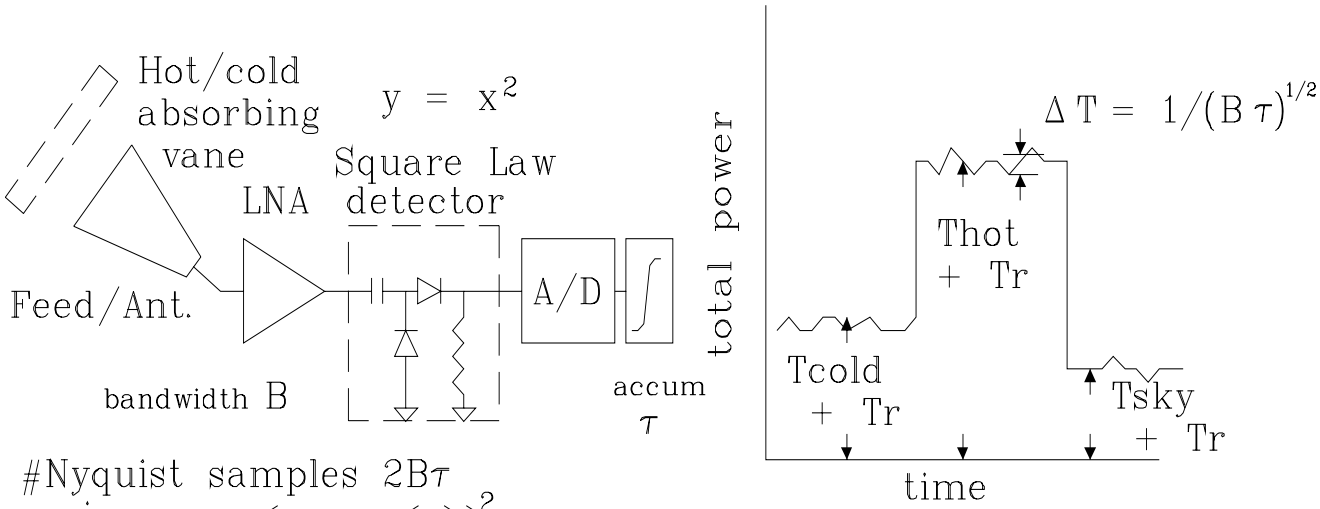

#Nyquist samples $2B\tau$

variance $= \langle y - \langle y \rangle \rangle^2$

$= \langle x^4 - 2x^2\langle x^2 \rangle + \langle x^2 \rangle^2 \rangle$

$= 3 - 2 + 1 = 2$ (from Gaussian RV)

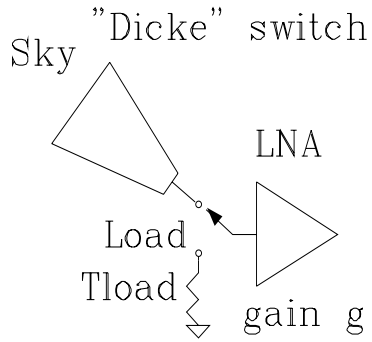

Psky = g(Tsky + Tr)

Pload = g(Tload + Tr)

Pcold = g(Tcold + Tr)

solve:

g = (Pload−Pcold)/(Tload−Tcold)

Tsky = (Psky−Pload)/g + Tload

Tr = Pload/g −Tload

(To make a spectrometer we add a filter bank, correlator + FFT, or FFT + square)

Radiometry and Spectroscopy

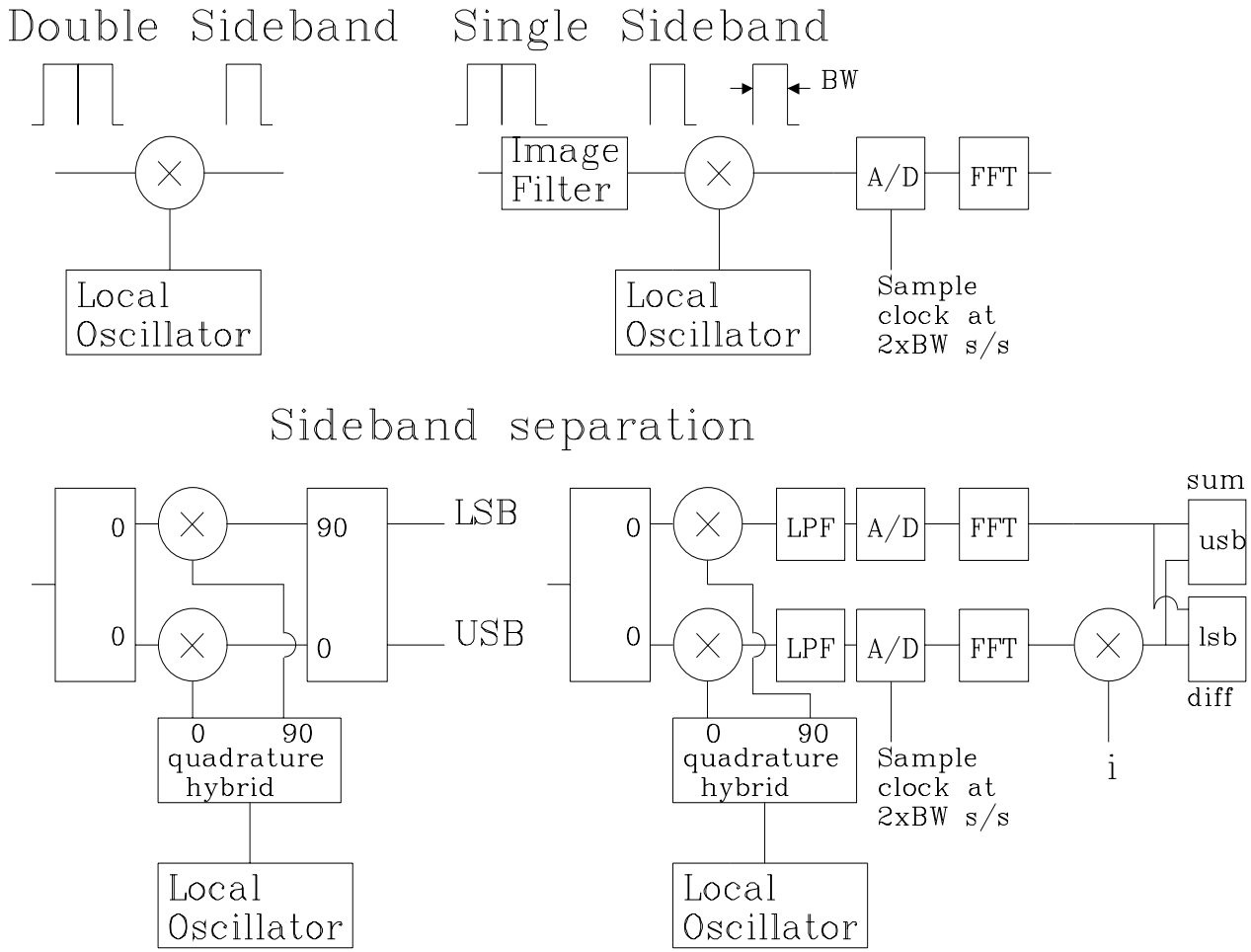

Frequency conversion “Superheterodyne” schemes

Low-Cost, Wideband MMIC Cryogenic LNA

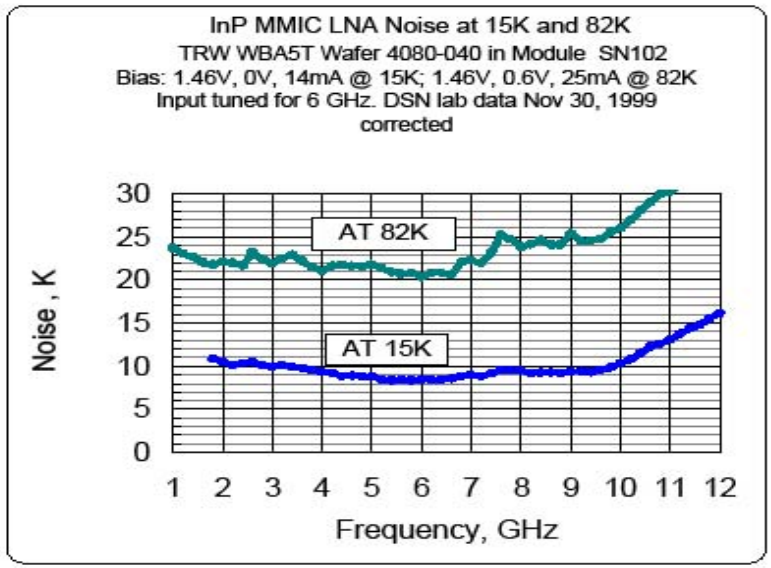

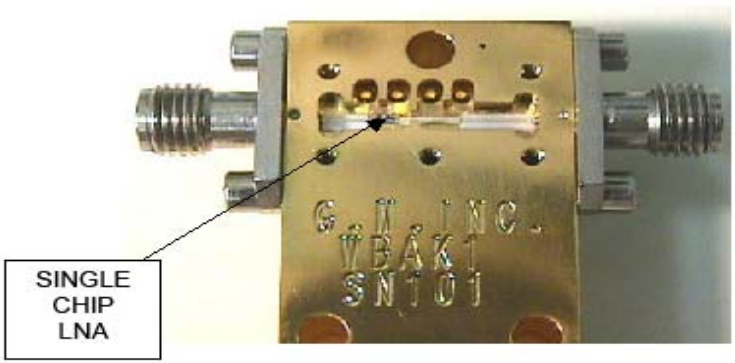

Development of wideband low noise amplifiers by Sandy Weinreb

Monolithic Integrated Circuit Very Low Noise 0.5 to 11 GHz Amplifier

Chip Size – 2mm x 0.74mm x 0.1mm, Material – Indium Phosphide

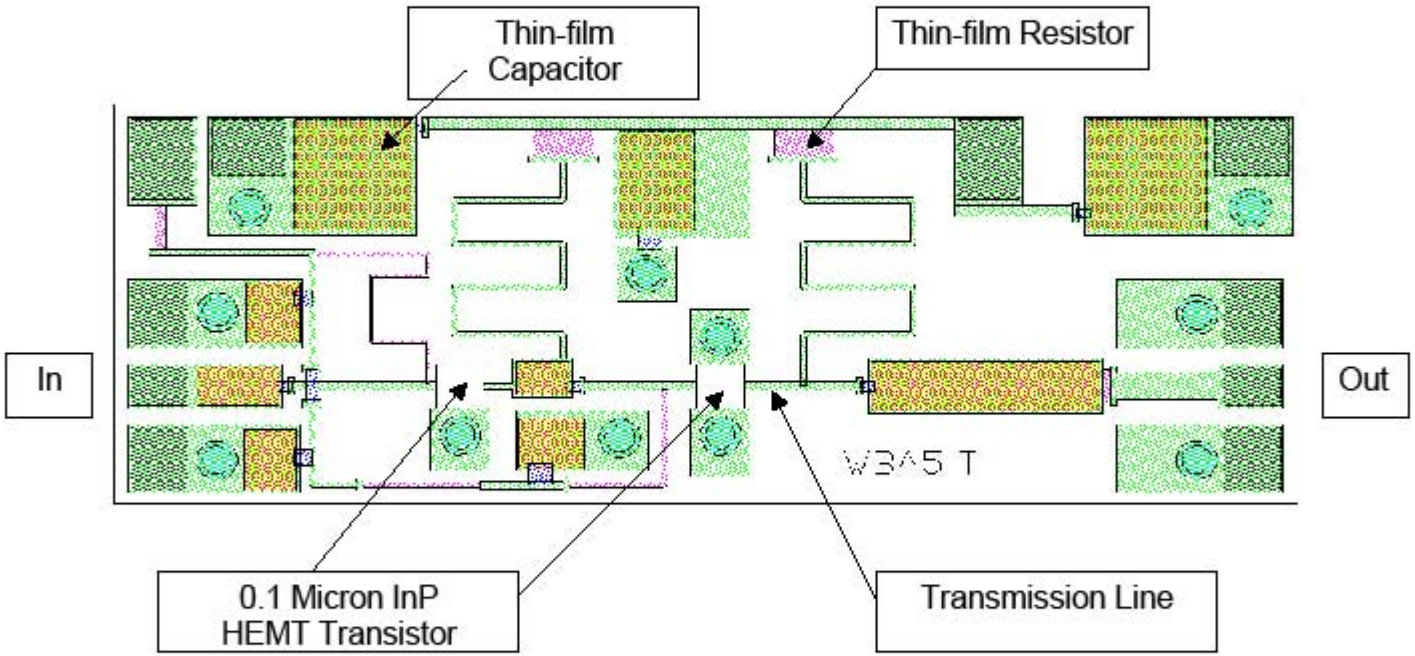

MMIC technology now in common use for Radio Astronomy

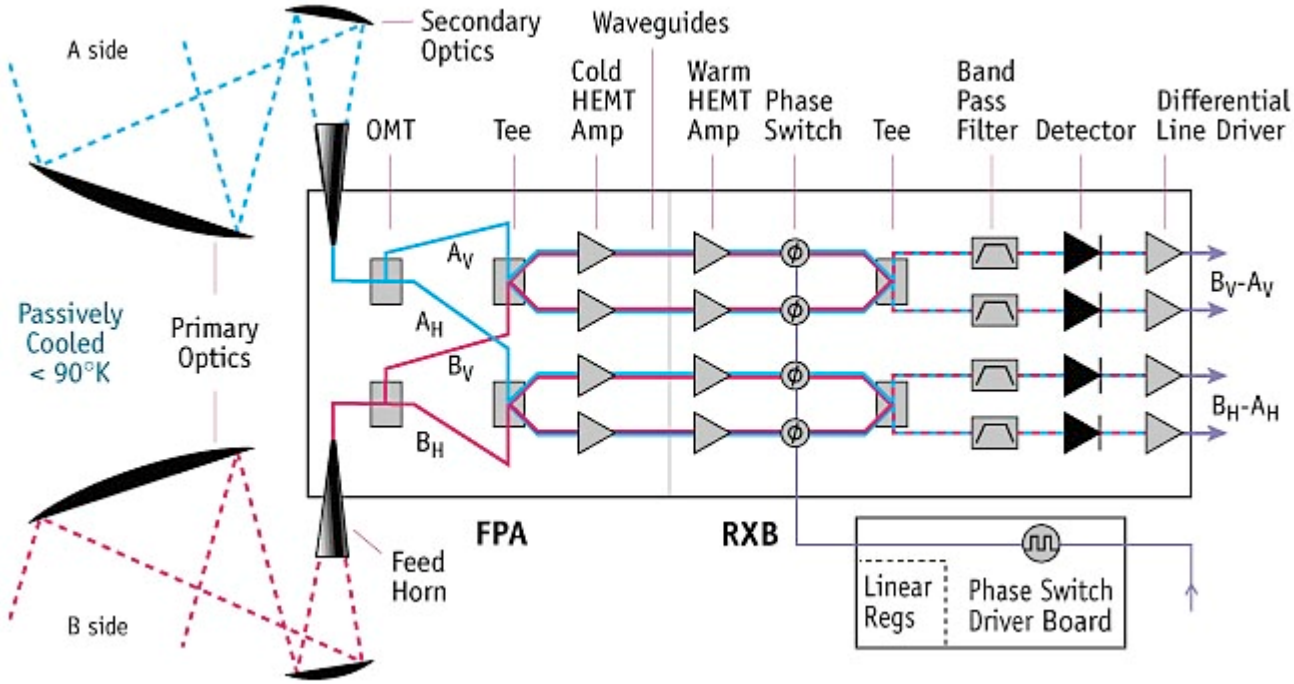

WMAP receiver “Dicke” switching scheme

Since the signals to be differenced are amplified by both amplifier chains, gain fluctuations in either amplifier chain act identically on both signals and thus cancel upon differencing.
The phase switches introduce a 180 degree relative phase change between the two signal paths, thereby interchanging which signal is fed to which square law detector. Thus, low frequency noise from the detector diodes is common mode and also cancels, further reducing susceptibility to systematic effects.

VSRT spectrometer as it was outside my office prior to moving to Chelmsford High School as part of an educational outreach project in January 2008

Spectroscopy processing:

$$x(t) \overset{FFT}{\leftrightarrow} X(\omega)$$

auto−correlation spectrum

$$\langle x(t)x(t-\tau)\rangle \overset{FFT}{\leftrightarrow} X(\omega)X^*(\omega) = S(\omega)$$

Note: window functions can be added for improved resolution functions

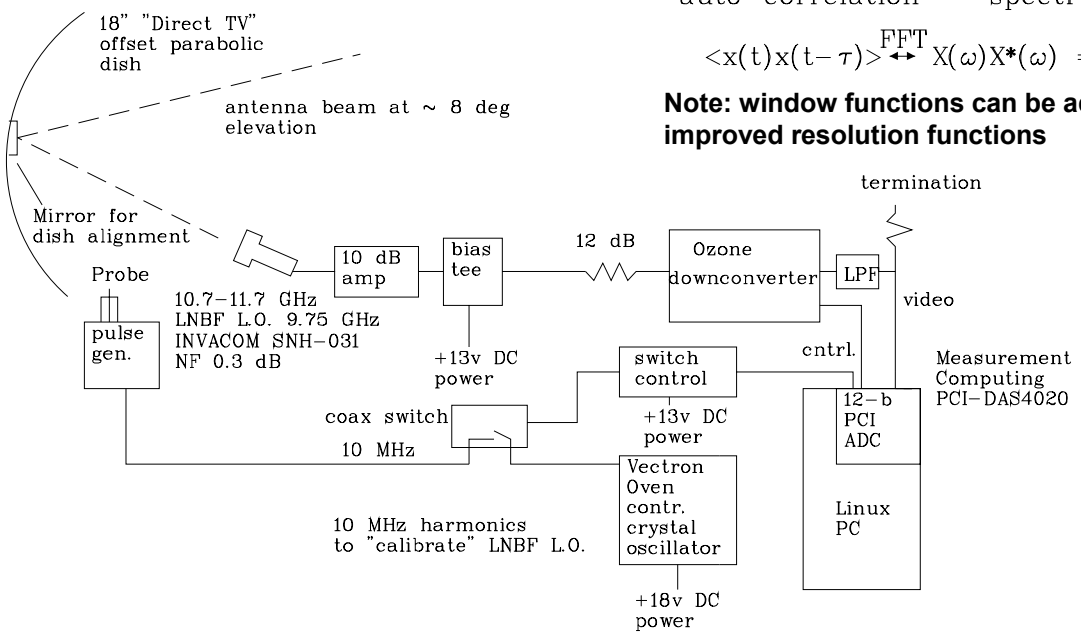

Setup to observe the 11.0724545 GHz ozone line

Very Small Radio Telescope (VSRT) Ozone Spectrometer

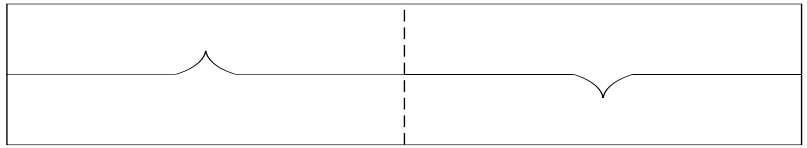

Frequency switching the LO puts the spectrum in the first half and then the second half of the bandpass

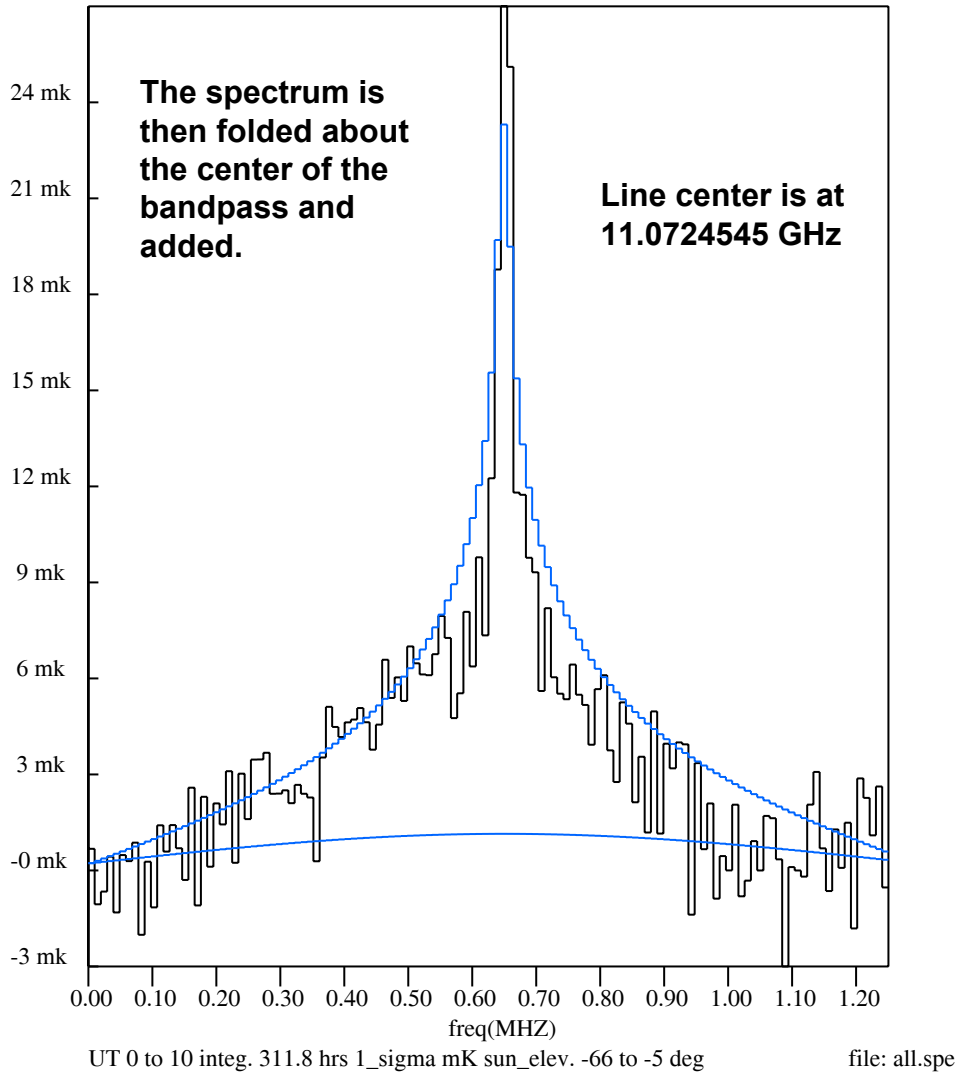

Ozone spectrum obtained using frequency switching

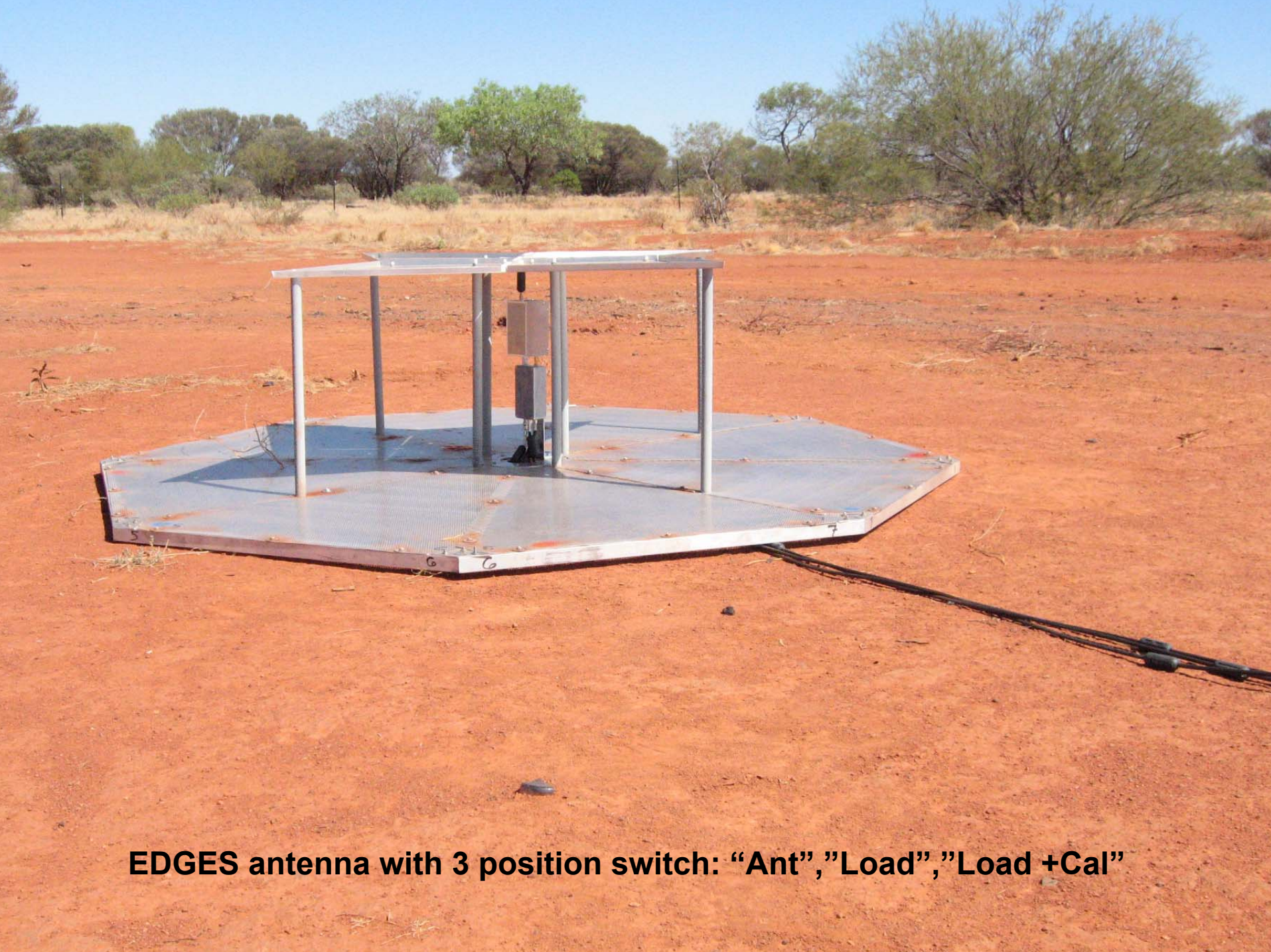

EDGES antenna with 3 position switch: “Ant”,”Load”,”Load +Cal”

Sky noise spectrum measured at Mileura in Western Australia. The data was taken in order to set a limit on the strength of 21 cm emission from the early universe. Details are reported by Bowman, Rogers and Hewitt in Ap.J. 2008, 676,pp 1-9

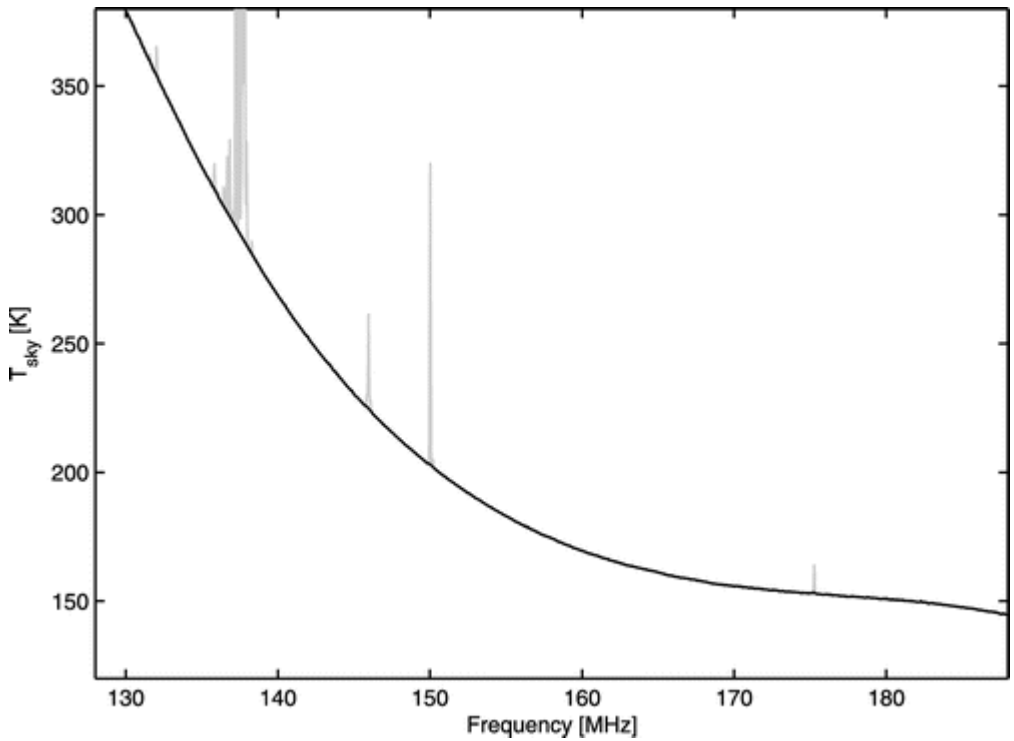

Sky noise spectrum

Fig. 3.— Integrated spectrum used for upper limit analysis of the reionization signal. The sky temperature, $T_{\mathrm{sky}\,}$, is an estimate based on modeled values for cable losses with no correction for antenna reflections. The spectrum represents the best 10% of the data from observations over two nights. It is selected by discarding individual observation cycles (see § 3.3) containing periods of particularly intense RFI. A total of approximately 1.5 hr of integration is included (3.75 hr including the ambient load and calibrator noise source measurements in each cycle). The black curve shows the spectrum after de-weighting the interferers (gray lines) present in the retained observations.

The results were limited by systematics because, while “Dicke” switching was used the systematics from the spectrometer only cancel completely when the “signal” and “comparison” spectra have almost equal shape at strength.

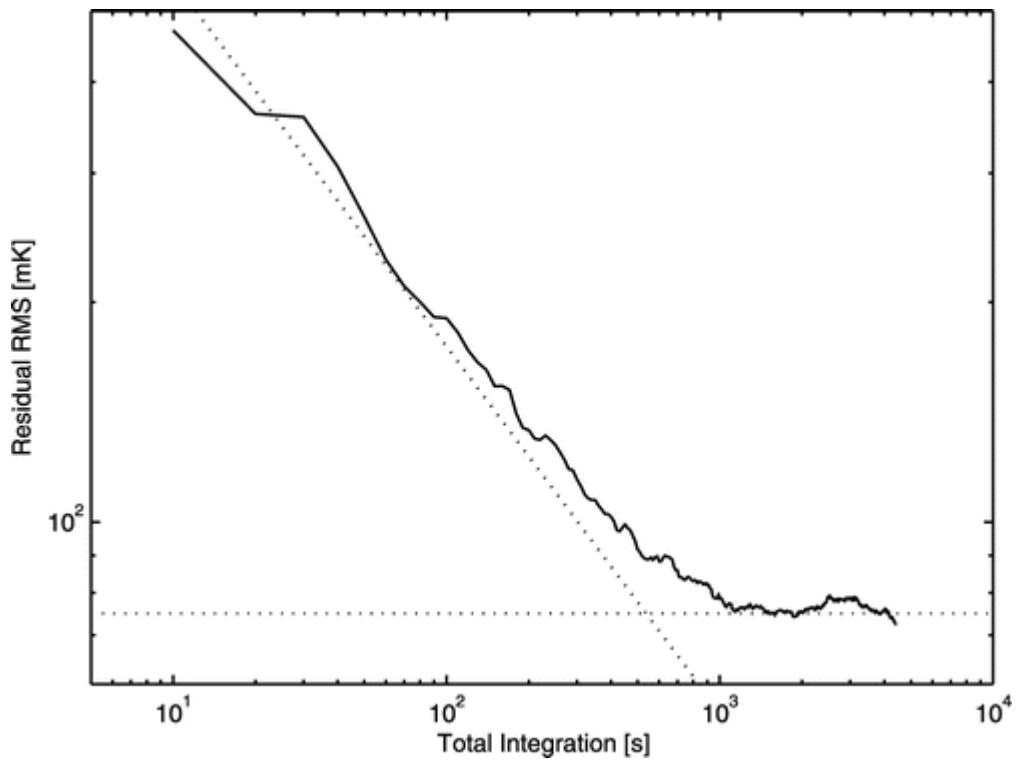

Noise goes down 1/sqrt(t) until systematics dominate

Fig. 5.— Characteristic amplitude of the residuals to the polynomial fit as a function of integration time on the sky. The rms follows a thermal $(b\tau) ^{-1/ 2}$ dependency until saturating at a constant 75 mK noise level due to the instrumental errors introduced into the measured spectrum. The dotted lines are guides for the eye showing a $(b\tau) ^{-1/ 2}$ profile and a constant 75 mK contribution.

The systematics in the digital direct sampling spectrometer used are mosly the result of coupling of the digital signals, like the FPGA clock, back into the analog to digital converter. Future development of spectrometers of this type require better isolation of the ADC from the other signals on the FPGA board.

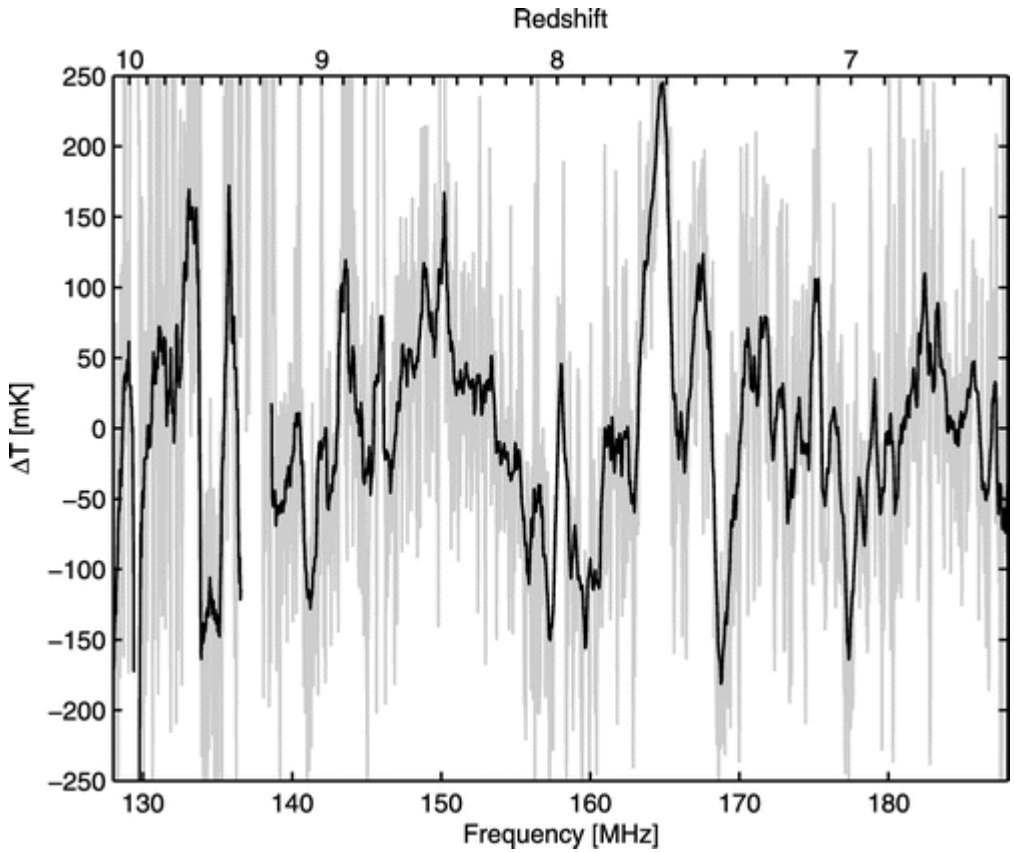

EDGES systematics

Fig. 4.— Residuals after subtraction of seventh-order polynomial fit to the measured spectrum shown in Fig. 3. The gray line is the raw spectrum with 122 kHz resolution. The black line is the spectrum after smoothing to 2.5 MHz resolution to reduce the thermal noise to below the systemic noise. The rms of the smoothed fluctuations is approximately 75 mK (see Fig. 5).

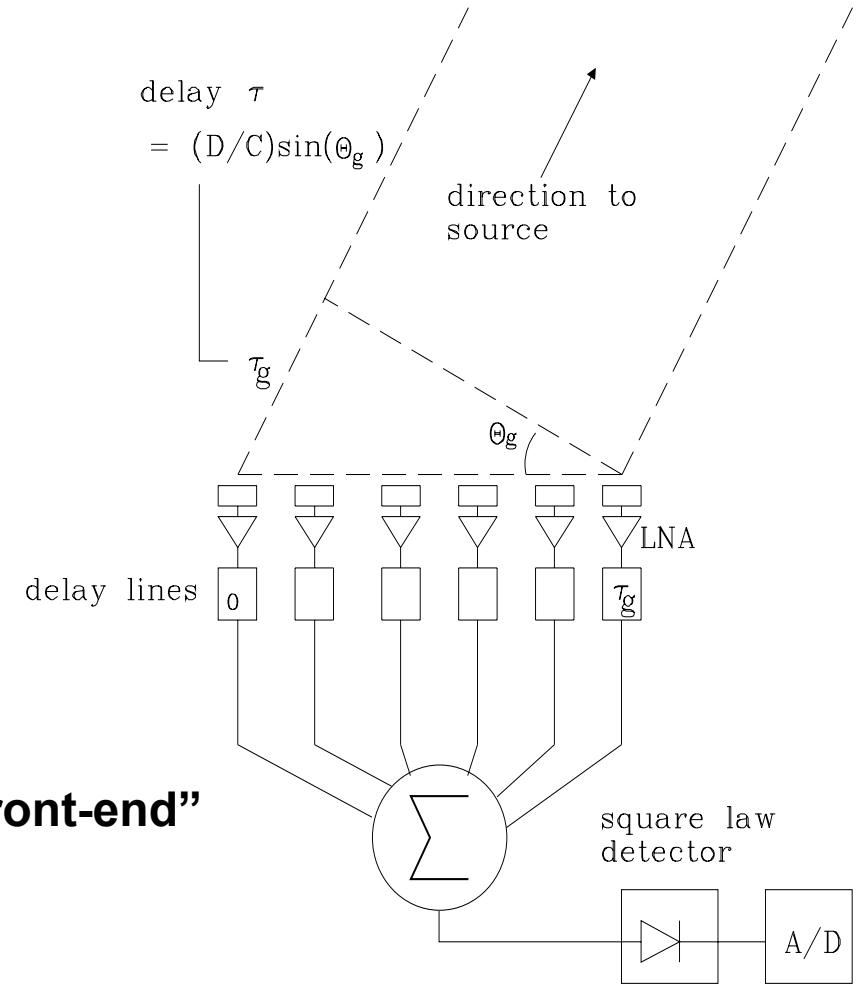

“front-end”

“back-end”

Simple “Beamformer”

Beamforming antennas come in many different configurations:

Digitization of each element as in the Deuterium array allows multiple beams to be formed simultaneously.

Backends can be simple total power detectors, spectrometers and/or data storage and transmission systems for the larger array as in the MWA

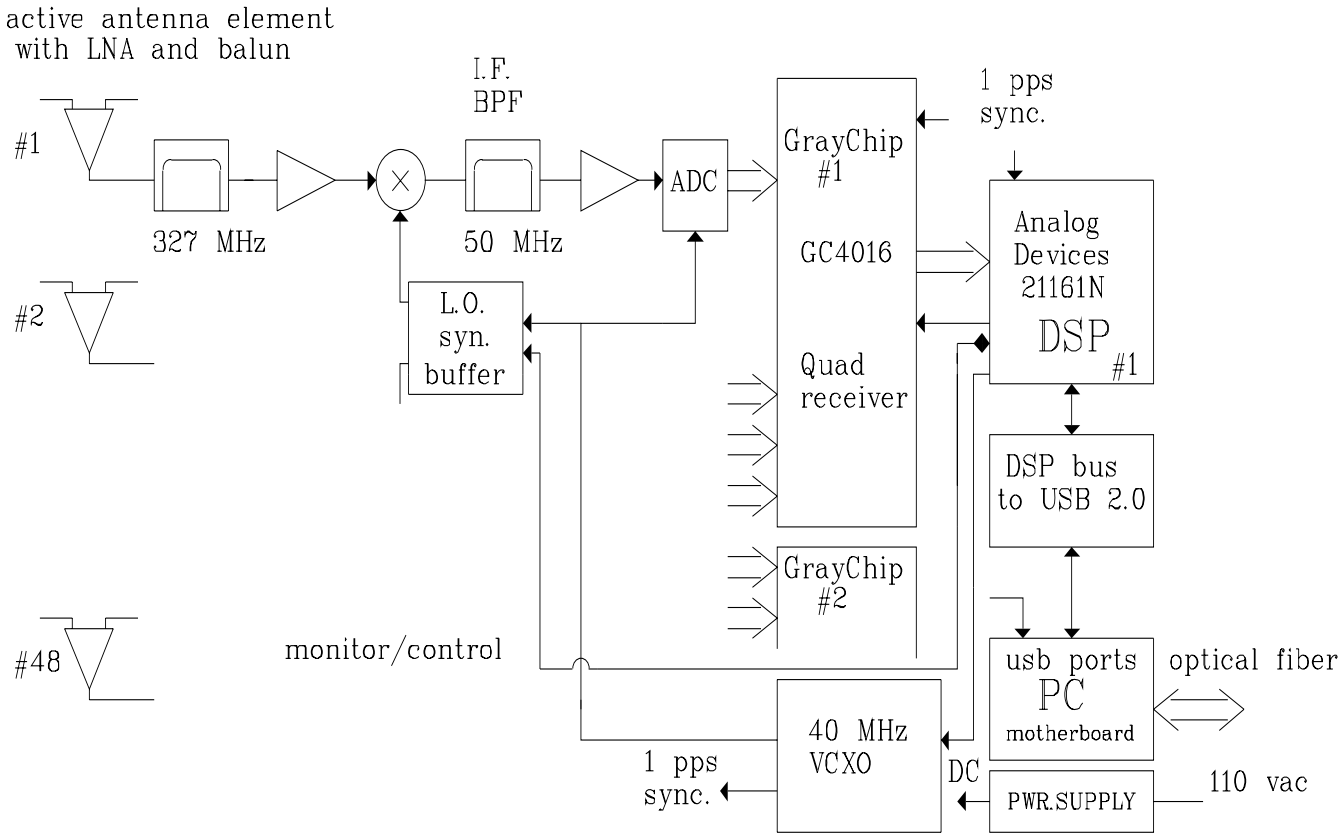

The data from each element is bandpass filtered in the GrayChip and then a FFT is taken in the DSP. Beamforming of the spectra is performed in the PC

Block diagram of Deuterium array station electronics

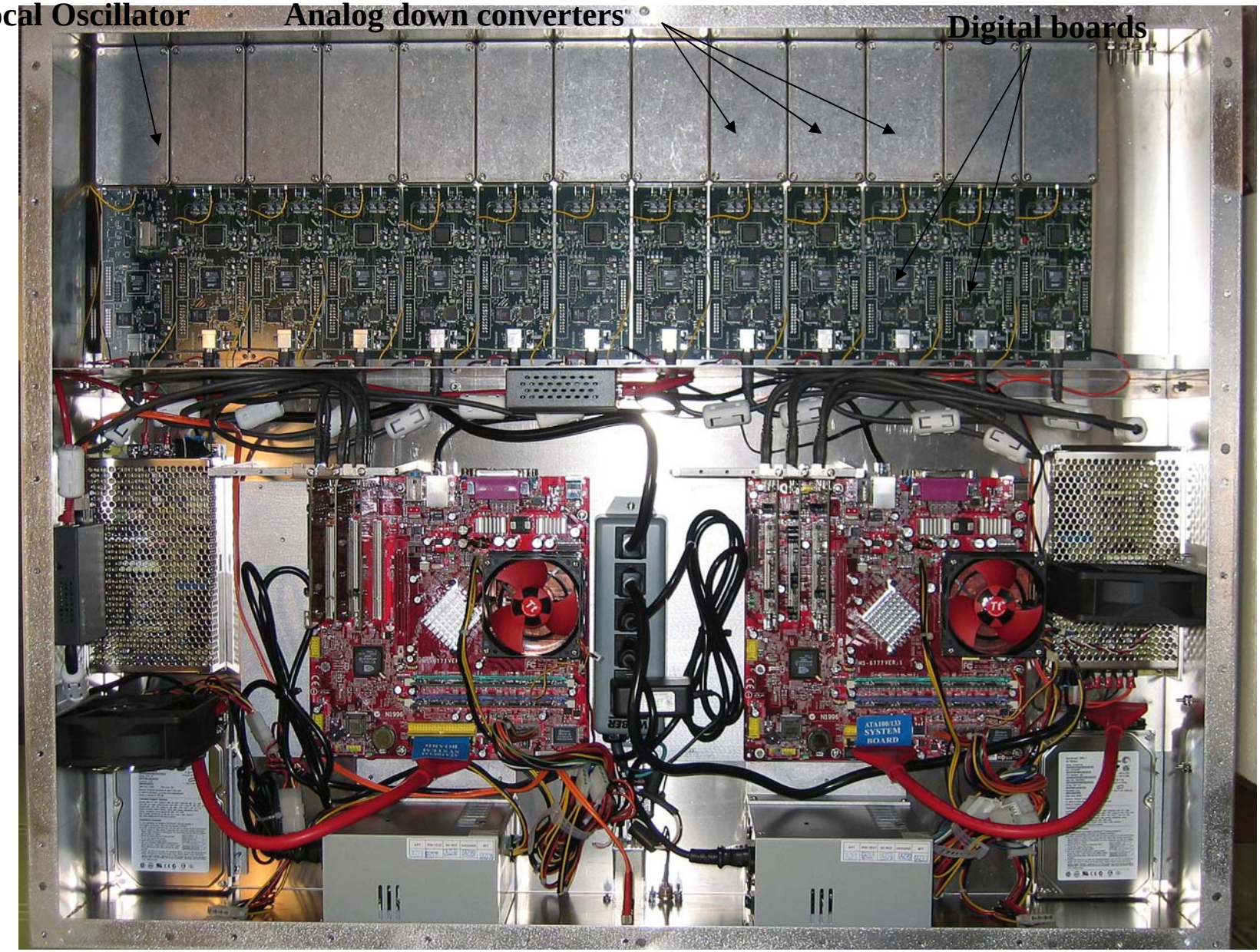

48 channel receiver for each station of the array – shown with cover removed

Details can be found in Rogers et al. 2007, A.J.,133,1625-1632

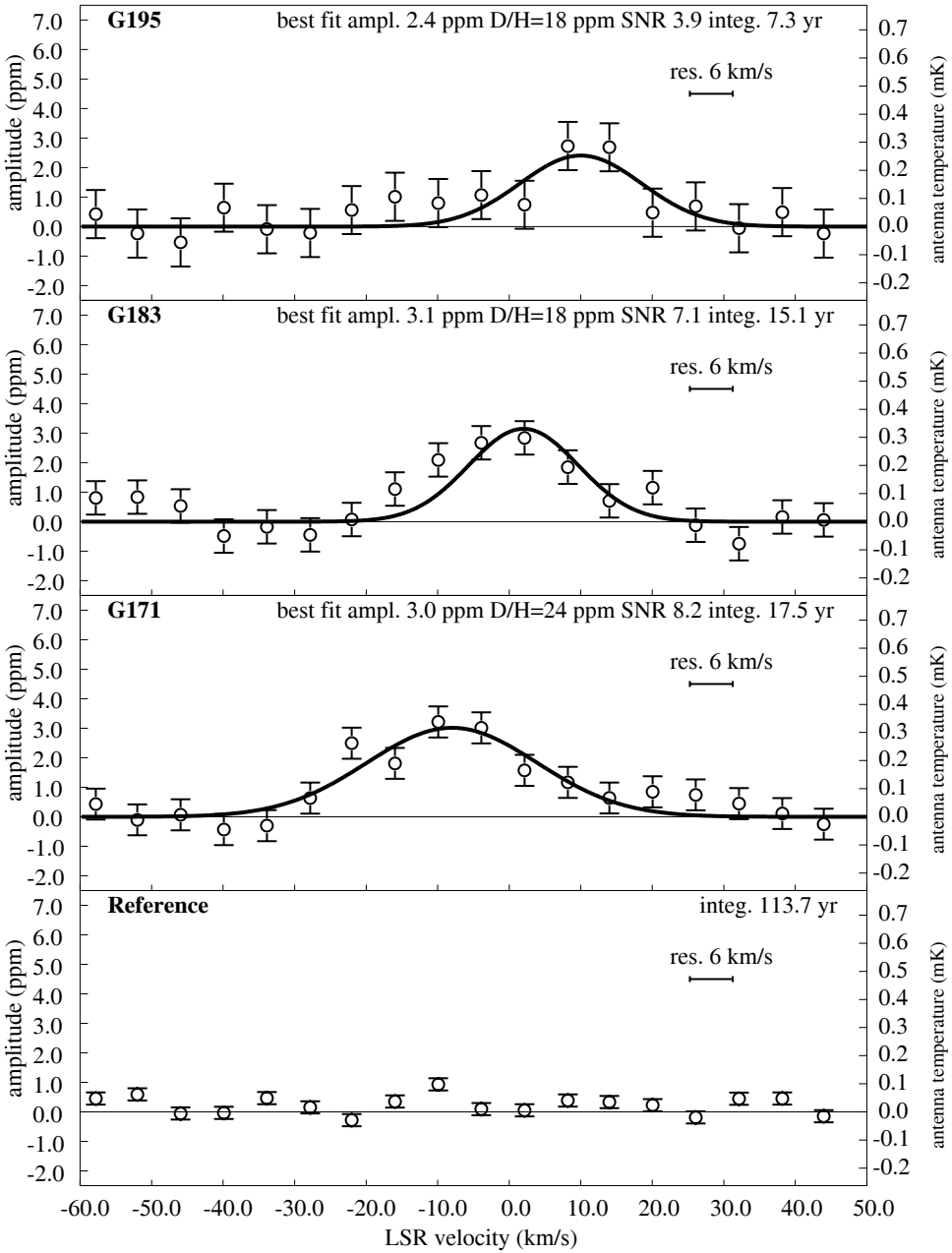

Spectra of the 327 MHz line of Deuterium in the Galactic anticenter from very long integrations using 24 beamforming stations

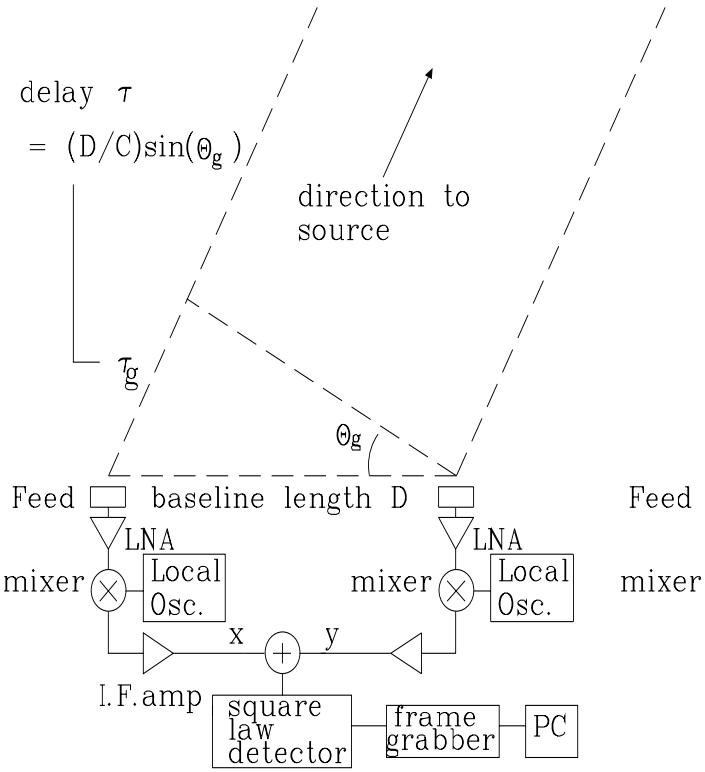

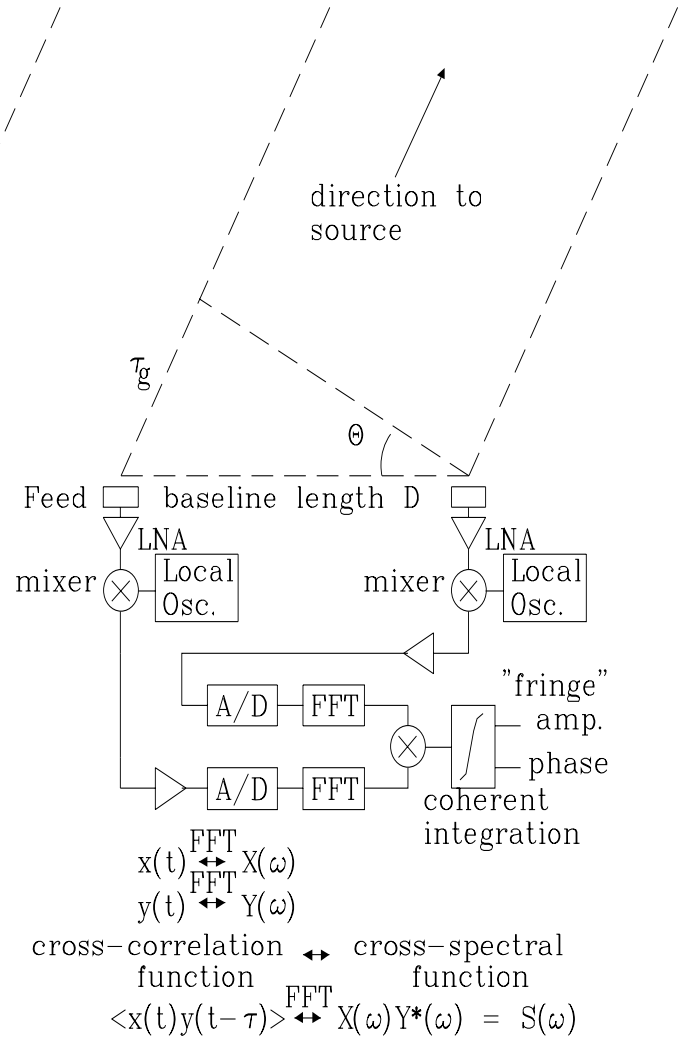

VSRT demonstrator **Single baseline interferometer**

INTERFEROMETRY

Note: Derivation of the rms noise requires Expectation product:

<abcd>=<ab><cd>+<ac><bd> +<ad><bc>

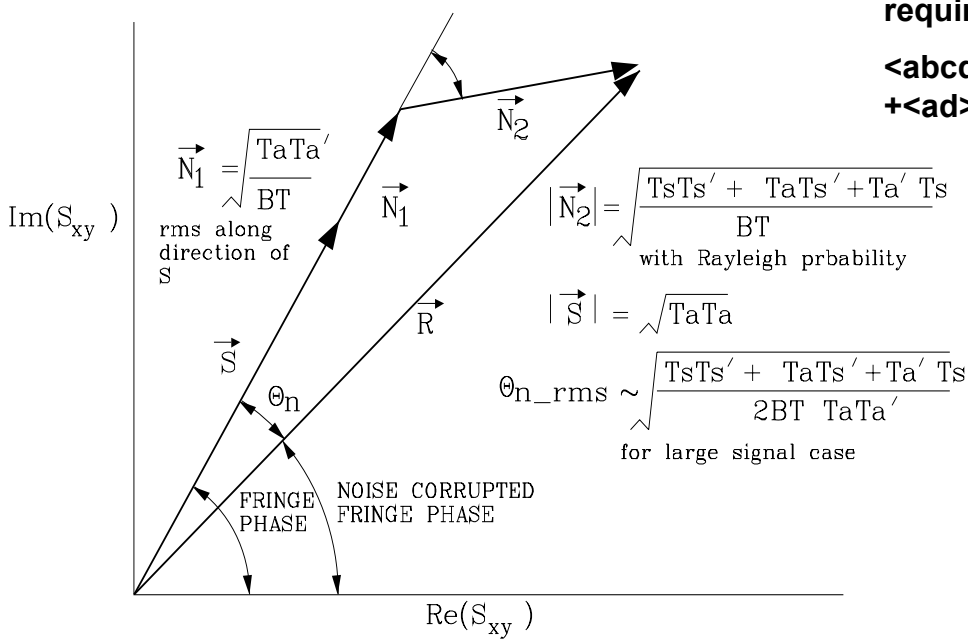

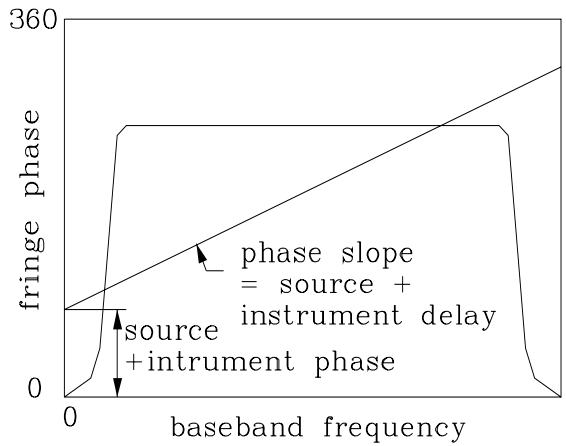

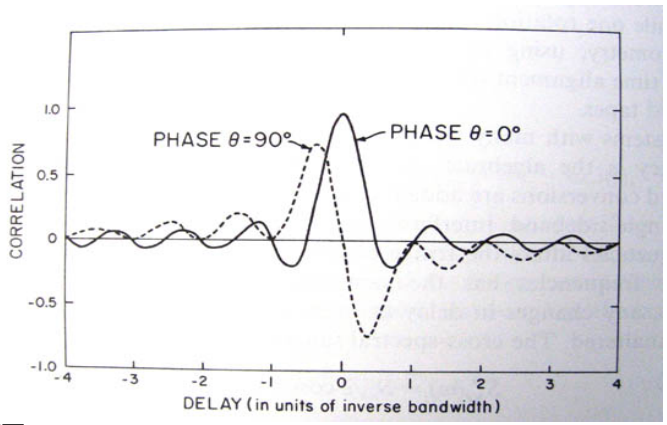

Frequency domain ⟷ **FFT** ⟷ **time domain**

Interferometer noise

See Interferometry and Synthesis in Radio Astronomy by Thompson, Moran and Swenson.

Very Long Baseline Interferometry (VLBI)

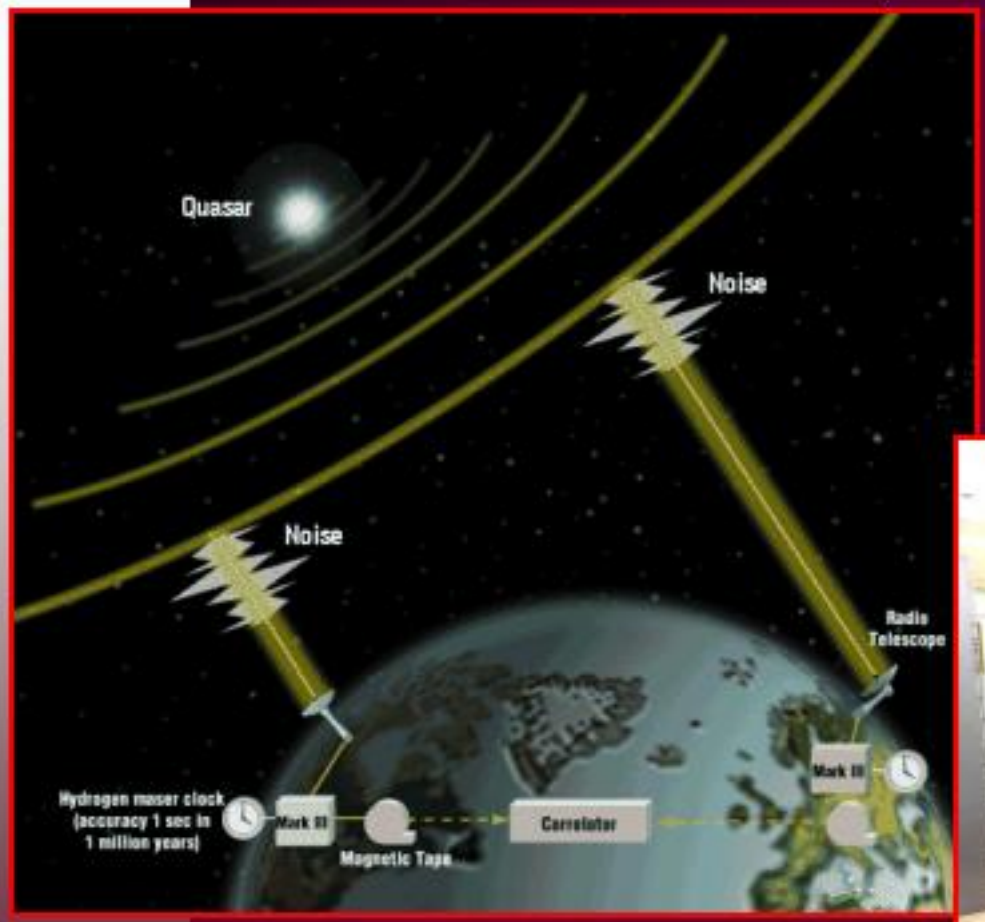

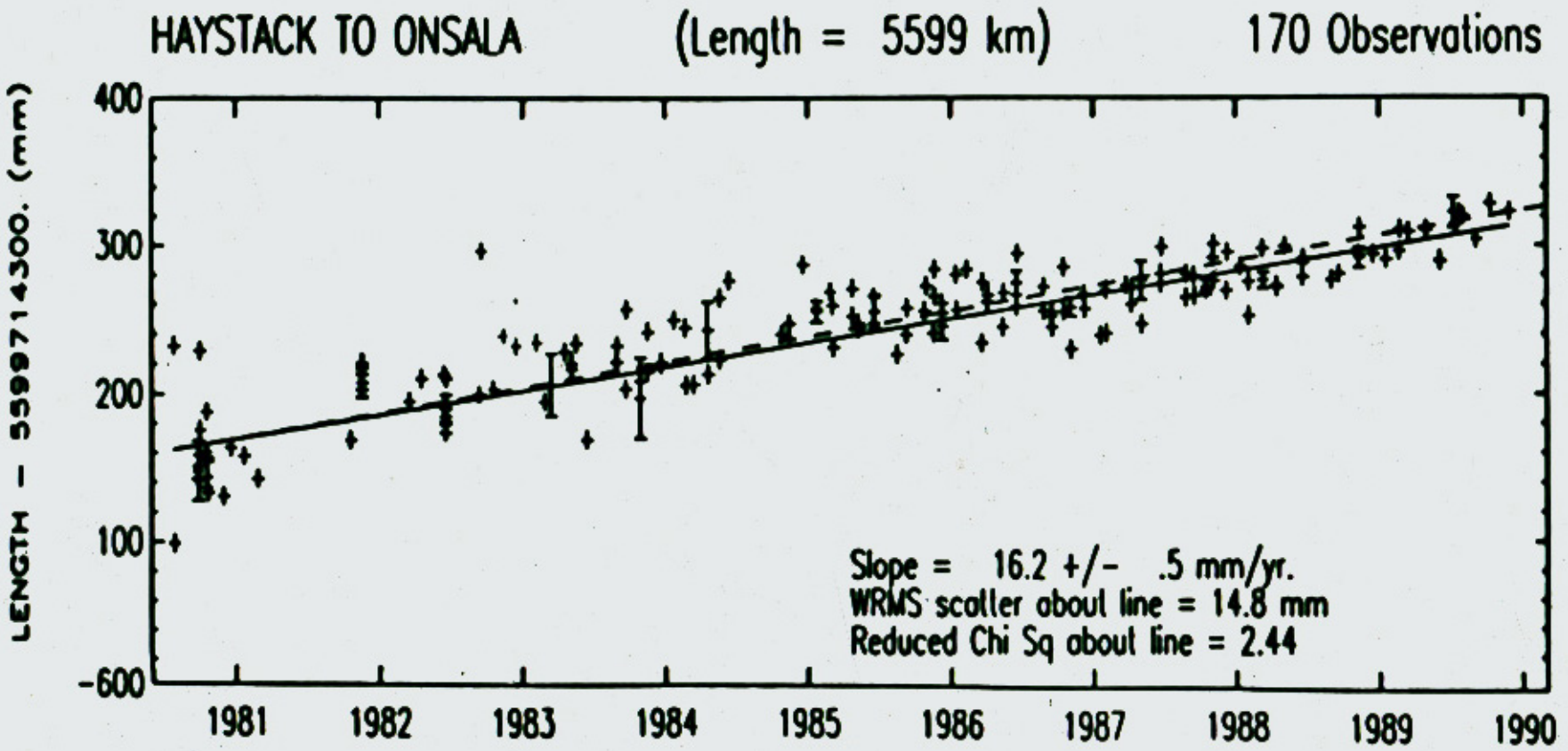

Measurement of interferometer delay (time difference of arrival) is the principle of geodetic VLBI

[The first direct evidence of tectonic plate motion came from VLBI]

"CLOSURE" QUANTITIES and "SELF"-CAL

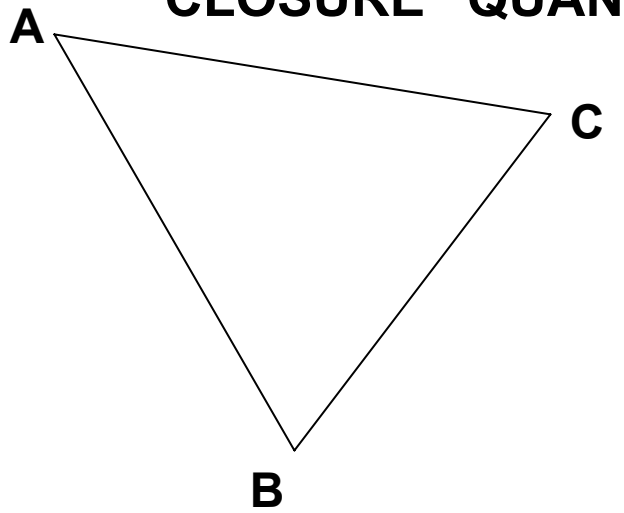

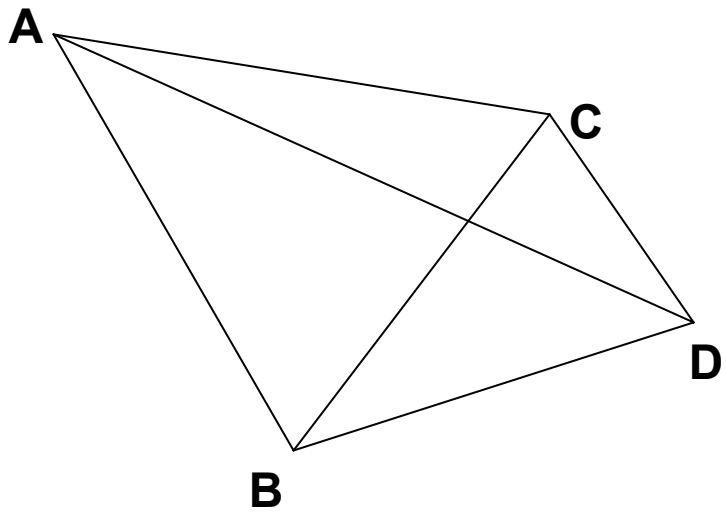

For a triangle of baseline:

"Closure phase" = $\Phi_{ab} - \Phi_{ac} + \Phi_{bc}$

For 4 stations:

"Closure amps" = (AB*CD)/(AC*BD)

(AB*CD)/(AD*BC)

More general "self-cal":

#baselines = N(N-1)/2

#unkown LO + atmos phases = N-1

#unkown amps = N

For sparse array:

Sensitivity: SNR ~ $\sqrt{}$#baselines

~ N

If not coherent: ~ $\sqrt{}$(N/2)

and improves ~ $T^{1/4}$

[see Rogers, Doeleman and Moran 1995, AJ, 109, pp 1391-1401 for details of coherent and incoherent averaging of interferometer data.]

"Closure" or "self-cal" is used to remove the effects of the atmosphere.

Note that despite the large and rapid changes in the interferometer phases due to the atmosphere the closure phase which provides some information on the source structure is stable.

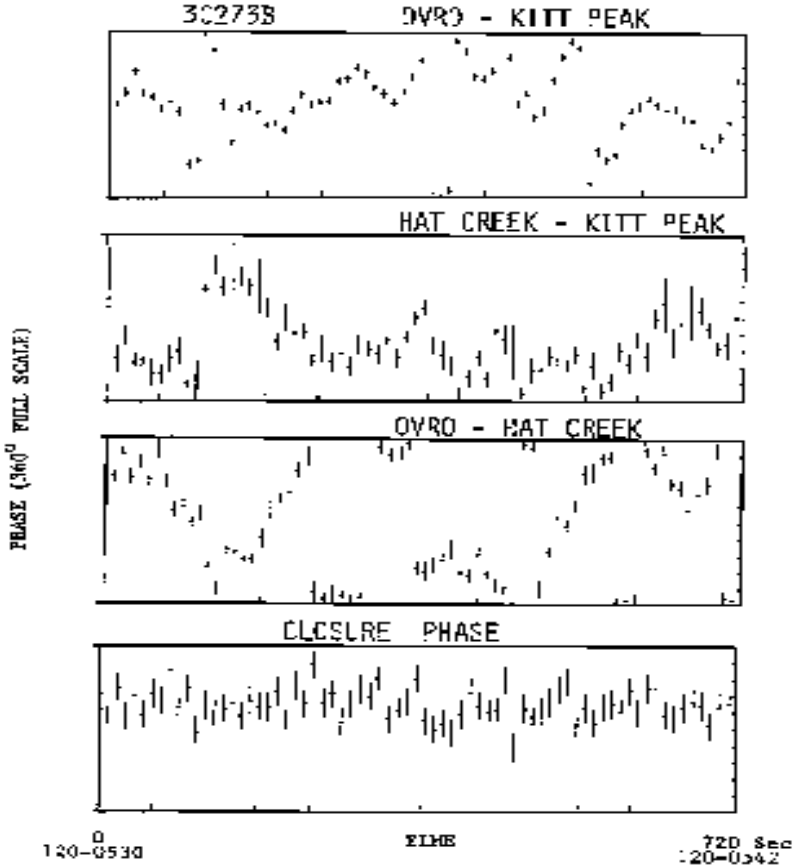

Fig. 5. Typical 89-GHz interferometer phases as a function of time from observations made in April 1983. The scan is 12 min long with phases shown for 10-s segments. The upper three curves are the phases on a triangle of baselines (OVRO, Hat Creek, and Kitt Peak), whereas the bottom curve shows the closure phases for this triangle.

ratio of each segment in units of the sigma noise level. The subtraction of 2 is needed to remove the bias that results from the noise. As long as the phase variations of the signal within each segment are small, the amplitude A will not be significantly reduced. Thus it is desirable to make the segments as short as possible to contain all the fringe energy while maintaining a reasonable signal to noise ratio for A. When the SNR for each segment is much greater than one, the SNR of A increases with the square root of N. In this case the incoherent averaging produces no significant loss in SNR when compared with coherent averaging. When the SNR of each segment is much less than one, a threshold proportional to the fourth root of N sets the detection limit. In this case the incoherent averaging process becomes relatively inefficient because the SNR will decrease with a reduction in segment length.

If fringes are detected on two baselines of a triangle, the coherent integration time can be extended on

Typical coherence of VLBI observations at 86 GHz

Note we could have used a measurement of the distance between the lamps at the null in the fringe amplitude along with the distance to the feeds to calculate the interferometer baseline, given the wavelength, or the wavelength given the baseline

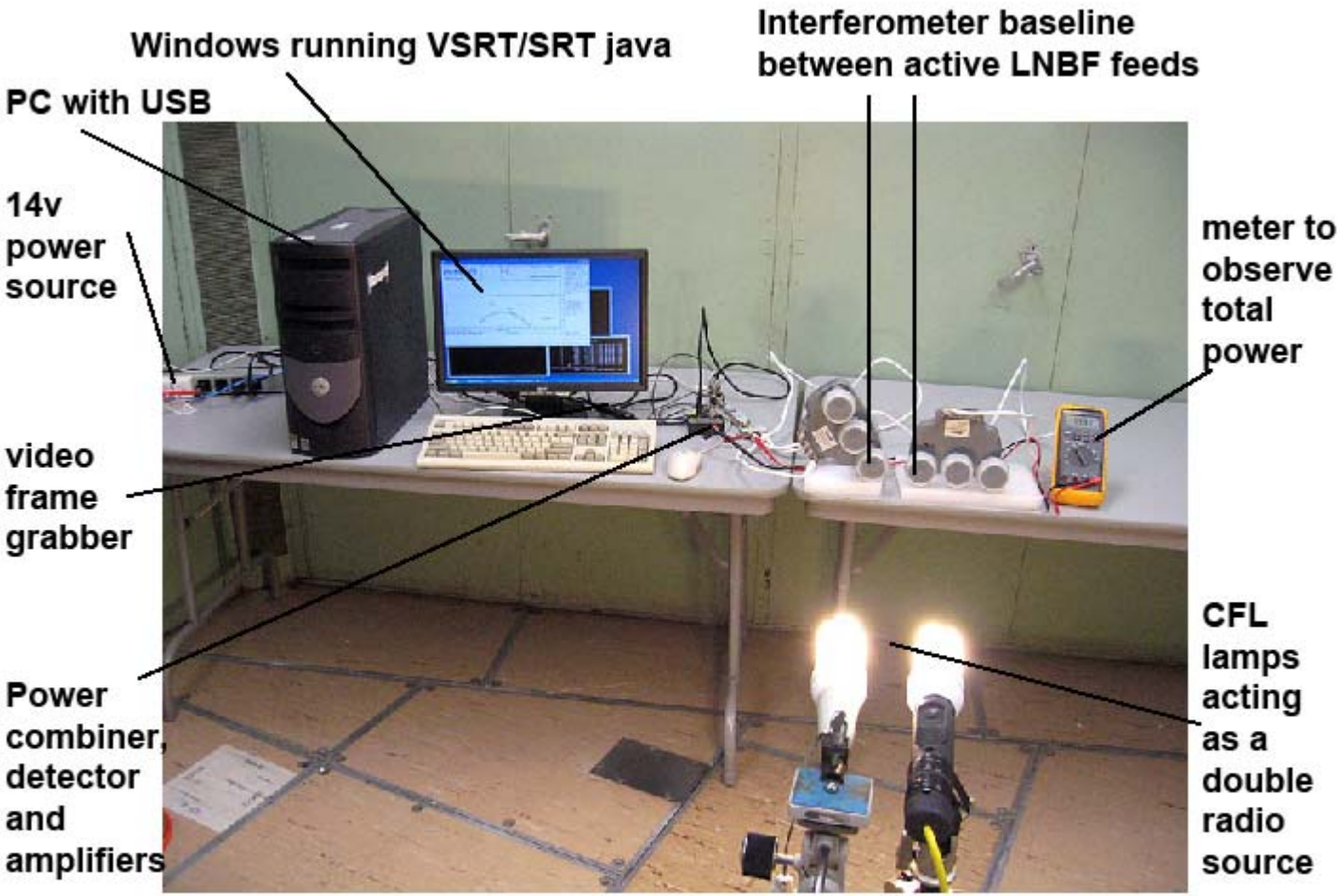

Simple laboratory setup to demonstrate the principles of radio interferometry

This simple double source experiment illustrates the principle used to obtain the results shown in the next slide.

to ~3. (iii) The estimates of the diameters and of the ratios of the flux densities of the components were not highly correlated with each other or with the estimates of either s or P. (iv) The estimate of P was within the interval 38 ± 2 deg for each experiment save that of 1972 April for which P could not be estimated accurately due to the shallowness of the observed fringe-amplitude minimum (thus, for the analyses of the 1972 April data, P was fixed at values between 36 and 40 deg). (v) The estimates of s varied nearly linearly with time, with the slope being (0.5 ± 0.1) milli-arcsec yr^{-1} (see Fig. 2) and negatively correlated with P. For example, the higher value of slope, 0.6 milli-arcsec yr^{-1}, is obtained with $P = 36$ deg, and the lower value, 0.4 milli-arcsec yr^{-1}, with $P = 40$ deg; for most of the experiments, the rms of the postfit residuals was smaller, by up to 15%, for $P \equiv 40$ deg than for $P \equiv 36$ deg.

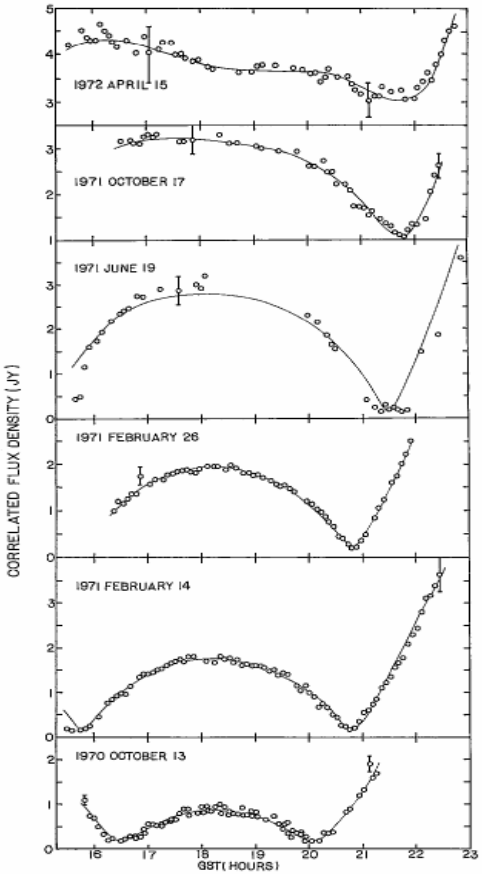

FIG. 1.—Correlated flux densities determined from VLBI observations of 3C 279 with the Haystack-Goldstone interferometer. (The u-v plane coverage for this interferometer is given by Whitney *et al.* 1971.) The error bars, given for typical observations, denote plus and minus one standard deviation. The solid curves are based on a parametrized, two-component model (see text).

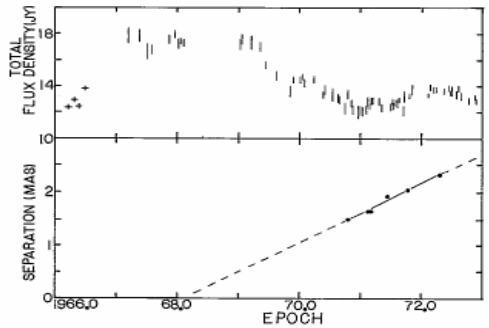

FIG. 2.—The estimated separation for each VLBI experiment of the two components of the model used to represent the compact part of the radio brightness distribution of 3C 279. The position angle assumed was 38° (see text). The straight line was determined by least squares. Also shown are the extrapolation to the time of zero component separation and the total flux densities observed at X-band for this entire period (a plus sign denotes the data from Aller 1970, and a vertical bar denotes the data from Dent and Kojoian 1972 and from Dent and Kapitsky 1976).

Thus, for P between 36 and 40 deg, the value of $\dot{s}$ corresponds to an apparent velocity v_a of separation of the two components of $v_a = (21 \pm 4)c$ for $z = 0.54$, $H_0 = 50$ km s^{-1} Mpc^{-1}, and $q_0 = 0.05$, with no allowance being made for the uncertainties in z, H_0, and q_0. Extrapolation backward in time indicates that the two components would have appeared to coincide in 1968.0 (+0.5, −0.7) as shown in Figure 2. Also displayed in Figure 2 is the available history for 3C 279 of the total flux density measured at radio frequencies near 8 GHz. An examination of these measurements, as well as those obtained at higher radio frequencies (see, for example, the compilation in Whitney *et al.* 1971), appears to indicate that a 1968.0 epoch is not a particularly special one with regard to the time variations of the total flux density of 3C 279.

IV. DISCUSSION

How can the apparent expansion rate of (21 ± 4)c be reconciled with the (10 ± 3)c result reported earlier by Whitney *et al.* (see also Cohen *et al.* 1971) on the basis of only the 1970 October and the 1971 February data? The reconciliation is effected by three factors:

Note that the null in the visibility amplitude (or "fringe amplitude" as it is often called) is the same effect as we saw in the VSRT demonstration illustrated in the previous slide.

"Superluminal" motion in the Quasar 3c279 from single baseline VLBI

3c279 is modeled as a simple double source

Some questions related to this presentation

Calculate the sensitivity of a 2 antenna radiometer observing a point source in the following configurations:

1] Using single antenna non-switched total power mode

2] "Dicke" switching between the 2 antenna (i.e. one as a reference and not pointed at the source)

3] Dividing the power to feed 2 LNAs, phase switching, recombining and using 2 square law detectors as in a single radiometer of the WMAP

4] Dividing the power from the antenna pointed at the source to feed 2 LNAs and then multiplying the outputs of the LNAs (i.e. a "correlation" receiver)

5] Configure the 2 antennas as a single baseline interferometer (with both antennas pointed at the source) and correlate the outputs of the LNAs

Ignore systematics and assume:

Tsys = 29 K, BW = 4 GHz (i.e. WMAPs 23 GHz radiometer)

Quote your results for the one sigma noise in units of mK $sec^{1/2}$

(for a single WMAP 23 GHz radiometer you should get 0.65 mK $sec^{1/2}$)